Molecular Vision 2026; 32:421-433 <http://www.molvis.org/molvis/v32/421>
Received 19 July 2025 | Accepted 25 September 2026 | Published 20 September 2026

© 2026 Molecular Vision

Activation of thioredoxin system, HIF-1a and pro-ferroptotic pathways by oxidative stress in human iPSC-derived retinal pigment epithelium cells

Anni Kolehmainen,[1] Robertas Čėsna,[2,3] Olga Vergun,[1] Dovilė Navicke,[2] Giedrius Kalesnykas,[1,2,4] Jenni J. Hakkarainen[1]

[1]R&D division, Experimentica Ltd., Kuopio, Finland; [2]R&D division, Experimentica UAB, Vilnius, Lithuania; [3]State Research Institute Centre for Innovative Medicine, Vilnius, Lithuania; [4]Department of Ophthalmology, Faculty of Medicine and Health Technology, Tampere University, Tampere, Finland

Purpose: Oxidative stress is a key factor in the development of age-related macular degeneration. In this study, the activation of the thioredoxin system in response to exogenous oxidative stress in retinal pigment epithelium cells derived from human induced pluripotent stem cells was demonstrated.

Methods: Oxidative stress was induced either by sodium iodate ($NaIO_3$) or *tert*-butyl hydroperoxide. Cell viability, reactive oxygen species (ROS) production, and vascular endothelial growth factor A (VEGFA) release were measured. Gene expression of *VEGFA*, hypoxia inducible factor 1 subunit alpha (*HIF1A*), thioredoxin (*TXN*) and thioredoxin-interacting protein (*TXNIP*), gamma-glutamylcyclotransferase 1 (*CHAC1*), and cystine/glutamate antiporter (*SLC7A11*) was determined.

Results: ROS levels significantly increased at the lowest $NaIO_3$ concentrations without a decrease in cell viability. Increased $NaIO_3$ induction resulted in significant upregulation of *VEGFA*, *HIF1A*, *TXN*, *CHAC1*, and *SLC7A11* and downregulation of *TXNIP* gene expression. Antioxidant treatment with Mn-TM-2-PyP significantly reduced $NaIO_3$-induced cytotoxicity, as indicated by decreased lactate dehydrogenase leakage, and helped to restore gene expression toward baseline levels.

Conclusions: $NaIO_3$ induction altered the expression of *VEGFA*, *HIF1A*, *TXN*, *TXNIP*, *CHAC1*, and *SLC7A11*, highlighting pathways linked to cellular stress, angiogenesis, and pro-ferroptotic events. These biomarkers provide actionable targets for testing antiangiogenic therapies (e.g., anti-VEGF drugs) and gene-editing therapies.

Retinal pigment epithelium (RPE), a highly specialized and polarized monolayer of cuboidal epithelial cells, is a part of the retina that has a crucial role in maintaining proper visual function and normal physiology of the eye [1]. RPE cells, which are connected by tight junctions, form the outer blood-retinal barrier together with Bruch's membrane, regulating the transport of molecules and metabolites between the neural retina and choroidal blood vessels [2]. The RPE is essential for maintaining the proper function and survival of the photoreceptors by processes such as phagocytosis of photoreceptor outer segments and light absorption [3].

Damage to the RPE and its function has been linked to the development of several diseases causing irreversible vision loss and blindness, such as age-related macular degeneration (AMD), which is the leading cause of blindness in the elderly in the Western world [4,5]. AMD can be divided into dry AMD, which is characterized by RPE dysfunction and macular geographic atrophy, and wet AMD, in which new blood vessels grow into the retina, leading to its detachment from the choroid [6,7]. This neovascularization is induced by vascular endothelial growth factor A (VEGFA), an angiogenic growth factor secreted by the RPE [8].

Oxidative stress, which may lead to cell damage caused by reactive oxygen species (ROS), has been shown to play a central role in the pathogenesis of AMD due to its major influence on RPE dysfunction and degeneration [9–11]. The RPE's location between the neural retina and the choroid exposes it to an oxidative environment, and the RPE is also constantly exposed to visible light, which leads to photo-oxidative stress [12,13]. In addition, the RPE is enriched in mitochondria due to its high metabolic demand, and mitochondria are a major source of ROS [14]. ROS production increases in aging and damaged cells. This leads to a harmful and amplified cycle of oxidative stress that results in the death of RPE cells and impairments in vision [3,15].

The thioredoxin system, an antioxidant pathway that plays a key role in regulating oxidative stress, is modulated by thioredoxin-interacting protein (TXNIP), an essential regulator of redox homeostasis. TXNIP inhibits thioredoxin

Correspondence to: Jenni J. Hakkarainen, R&D division, Experimentica Ltd., P.O. Box 1199, FI-70211 Kuopio, Finland, email: jenni@experimentica.com

by forming a mixed disulfide bond with its active site thiols, thereby suppressing its antioxidant function [16,17]. Studies have shown that TXNIP also interacts with various other proteins and systems. Upon transient exposure to physiologic levels of hydrogen peroxide or tumor necrosis factor, TXNIP activates signaling via vascular endothelial growth factor receptor 2 and triggers apoptosis [18,19]. TXNIP also plays a pivotal role in angiogenesis by interacting with hypoxia-inducible factor 1 alpha (HIF-1α) and facilitating its degradation [19,20]. These findings highlight TXNIP as a promising target for angiogenesis-related diseases such as AMD.

Oxidative stress is one of the main causes of RPE damage and cell death. Therefore, the study of its effects on the thioredoxin system's antioxidative and proangiogenic-related genes is pivotal for understanding the pathology and progression of AMD. Sodium iodate ($NaIO_3$) has been commonly used as an exogenously applied oxidative stressor, having significant effects on RPE cell dysfunction, damage, and viability in vitro [21,22] and in vivo [23]. However, in vitro data are primarily derived from cell lines, such as ARPE-19, which may not fully reflect the key characteristics of RPE. After the discovery of human induced pluripotent stem cell (hiPSC) technology in 2007 [24,25], RPE cells derived from hiPSCs have become an important in vitro tool to study RPE-based disease mechanisms, as they have been proven to express key functional and morphological attributes of native RPE [26]. Furthermore, information on hiPSC-RPE cell response to different oxidative stressors and how their intrinsic antioxidant systems are activated remains scarce in the literature.

The aim of this study was to demonstrate the effects of $NaIO_3$ induction in hiPSC-RPE cells and determine the activation of the thioredoxin system by measuring the changes in the expression of antioxidative and proangiogenic-related genes *VEGFA*, *HIF1A*, thioredoxin (*TXN*), and *TXNIP*. Furthermore, pro-ferroptotic events were evaluated by gene expression of oxidative stress–triggered ferroptosis mediator gamma-glutamylcyclotransferase 1 (*CHAC1*) and the cystine/glutamate antiporter (*SLC7A11*), which regulates ferroptosis by promoting cystine uptake and glutathione synthesis. In addition, we wanted to further characterize hiPSC-RPE cells to confirm their similarity to human RPE cells by immunocytochemistry to assess RPE-specific protein expression, visualizing cellular organelles and evaluating melanosome maturation stages with transmission electron microscopy, and assessing cell monolayer integrity with transepithelial electrical resistance (TEER) and permeability testing.

METHODS

Cell culture: The hiPSC-derived RPE cells (donor sex: male, population: Caucasian) were received at passage 2 from Phenocell (Grasse, France) and were cultured in RPE medium containing 70% Dulbecco's modified Eagle's medium, high glucose, 30% Ham's F12 Nutrient Mix, 2% B-27 supplement, and 1% antibiotic-antimycotic, all from Gibco, Thermo Fisher Scientific (Waltham, MA). Cells were used at passages 3 to 4 for experiments. Passaging of hiPSC-RPE cells was performed using Accumax solution (Sigma-Aldrich, St. Louis, MO), and cells were seeded on Matrigel (Corning, Corning, NY)–coated permeable Transwell cell culture inserts (Corning) and 96-well plates (μClear; Greiner Bio-One, Kremsmünster, Austria) at a density of 100,000 cells/cm^2. The cells were cultured on inserts for 28 days and in 96-well plates for 22 days at 37 °C, 5% CO_2. Cells tested negative for mycoplasma using MycoAlert (Lonza, Basel, Switzerland).

Immunocytochemistry: Cells cultured on inserts were washed with Dulbecco's phosphate-buffered saline (DPBS; Gibco, Thermo Fisher Scientific), fixed with methanol for 10 min, washed again, and blocked in blocking buffer (5% goat serum in DPBS) for 20 min. The membranes containing the cells were cut out from the inserts and transferred to a well plate. Cells were incubated in different primary antibodies, including anti–zonula occludens 1 (1:100; Thermo Fisher Scientific), anti-occludin (1:100, Thermo Fisher Scientific), anti-RPE65 (1:100; Novus Biologicals, Bio-Techne, Minneapolis, MN), and anti-ARL13B (1:100; Proteintech, Manchester, UK) for 90 min; washed with washing solution (0.5% goat serum in DPBS); and incubated in secondary antibody for 1 h. Secondary antibodies were goat anti-rabbit or anti-mouse IgG Alexa Fluor 488 (1:1,000; Thermo Fisher Scientific), and for ARL13B staining, the secondary antibody was excess Fab fragment goat anti-rabbit Alexa Fluor 594 (1:100; Jackson ImmunoResearch Europe Ltd, Cambridgeshire, UK). After washing, the cell nuclei were stained with 0.1 μg/ml 4′,6-diamidino-2-phenylindole (DAPI; Sigma-Aldrich) for 10 min. The cells were mounted on microscope slides using FluoroShield (Sigma-Aldrich). Images were acquired using a fluorescence microscope (Leica Microsystems GmbH, Wetzlar, Germany).

Transmission electron microscopy: Cells cultured on inserts were washed with DPBS, fixed with 2% paraformaldehyde and 0.5% glutaraldehyde for 10 min, and washed with 0.1 M phosphate buffer (pH 7.4). Cells were postfixed in 1% osmium tetroxide (Electron Microscopy Sciences, Hatfield, PA) for 1 h, washed, and dehydrated in a series of ethanol (50%, 70%, 96%, and absolute ethanol). An epoxy resin embedding kit

(Ladd Research, Williston, VT) was used for cell infiltration and embedding according to the manufacturer's instructions. Ultrathin sections (70 nm) were cut and stained with uranyl acetate and lead citrate (both from Electron Microscopy Sciences). Images were obtained with a JEM-2100F transmission electron microscopy (TEM) microscope (Jeol, Tokyo, Japan).

Transepithelial electrical resistance assessment: Culture medium was removed from the inserts, and cells were washed with warm Hank's Balanced Salt Solution (HBSS; Gibco, Thermo Fisher Scientific) with 25 mM HEPES (Sigma-Aldrich). After washing, the cells were balanced with the same buffer for 30 min at 37 °C, and TEER values were measured using an EVOM2 Epithelial Volt/Ohm Meter (World Precision Instruments, Sarasota, FL). After the permeability experiments, test solutions were removed, fresh buffer was added in the chambers, and TEER values were measured as described above.

Permeability testing: The permeability tests were performed in inserts from the basolateral to apical direction (i.e., representing transport from choroid to retina). Reference compounds were diluted in HBSS-25 mM HEPES solution, 6-carboxyfluorescein (100 µM), and rhodamine B (100 µM) from Sigma-Aldrich and placed in the donor chambers. Fresh buffer was added to the receiver chambers. The samples were taken from the receiver chambers at 10, 20, 30, 40, 50, and 60 min and from the donor chambers at 0, 30, and 60 min. The loss of volume in the receiver chambers was replaced with equal volumes of fresh buffer. The fluorescence intensity of the samples was measured using a Cytation 3 multimode reader (BioTek Instruments, Winooski, VT), and sample concentrations were determined using standard curves. Three independent experiments in duplicate were performed (n = 6).

Induction of oxidative stress: Oxidative stress was induced in hiPSC-RPE cells grown in 96-well plates with $NaIO_3$ in concentrations of 0 to 20 mM and *tert*-butyl hydroperoxide (tBHP) in concentrations of 0 to 1.2 mM (both from Sigma-Aldrich) at 37 °C for 24 h. $NaIO_3$ was diluted in RPE culture medium with B-27 supplement without antioxidants (Thermo Fisher Scientific).

Antioxidant treatment: To evaluate antioxidant-mediated suppression of $NaIO_3$-induced effects, cells were treated with manganese (III) tetrakis(1-methyl-4-pyridyl)porphyrin (Mn-TM-2-PyP, 0.005%), a cell-permeable antioxidant with broad redox activity, for 24 h before and during $NaIO_3$ exposure. The experiment involving antioxidant was conducted only once for demonstrative purposes, and the results should be interpreted as preliminary and considered directional rather than conclusive. Further replication is required to confirm these findings.

Lactate dehydrogenase and VEGFA release assays: Culture medium was sampled to assess lactate dehydrogenase (LDH) and VEGFA release from the hiPSC-RPE cells. LDH was measured as previously described [27]. VEGFA concentrations from the cell supernatants were measured using the Human VEGFA Quantikine ELISA Kit according to the manufacturer's instructions (R&D Systems, Bio-Techne, Minneapolis, MN). Three independent experiments (n = 3) were performed with four to eight technical replicates.

Resazurin cell viability and ROS assays: The reduction of resazurin to fluorescent resorufin was used to assess cell viability. Resazurin (Sigma-Aldrich) 0.01 mg/ml in HBSS was added to the cells, which were then incubated at 37 °C for 1 h. The formation of ROS was measured with a general oxidative stress indicator, CM-H_2DCFDA (Thermo Fisher Scientific), which was added to the cells at 5 µM in HBSS and incubated at 37 °C for 1 h (loading), after which the cells were incubated in HBSS at 37 °C for an additional 30 min. Fluorescence intensities were measured using the Cytation 3 reader. Three independent experiments (n = 3) were performed with two to four technical replicates. After the fluorescent measurements, cells were washed with DPBS and lysed in TRIzol reagent (Thermo Fisher Scientific).

RNA purification: $NaIO_3$-induced hiPSC-RPE cells were lysed in TRIzol reagent, and cells from 2 wells were pooled. Phase separation and RNA isolation were performed from the colorless upper aqueous phase with a PureLink RNA Mini Kit (Thermo Fisher Scientific) according to the manufacturer's instructions. Optional on-column PureLink DNase treatment was performed to minimize DNA contents in purified RNA samples. RNA concentration and purity were determined with a NanoDrop One^C Microvolume UV-Vis Spectrophotometer (Thermo Fisher Scientific).

Complementary DNA synthesis and real-time quantitative polymerase chain reaction amplification: Complementary DNA (cDNA) synthesis was performed with the High-Capacity RNA-to-cDNA Kit (Thermo Fisher Scientific) according to manufacturer's instructions using 0.2 µg total RNA from cells. Then, 5 ng cDNA samples were used for target (carboxyfluorescein [FAM]-labeled) and endogenous control (2′-chloro-7′phenyl-1,4-dichloro-6-carboxy-fluorescein [VIC]-labeled) gene quantitative polymerase chain reaction (qPCR) amplification with five different TaqMan assays: vascular endothelial growth factor A (*VEGFA*, Hs00900055_m1), hypoxia-inducible factor 1 alpha (*HIF1A*, Hs00153153_m1), thioredoxin (*TXN*, Hs00828652_m1), thioredoxin-interacting protein (*TXNIP*, Hs00197750_m1),

ChaC glutathione-specific gamma-glutamylcyclotransferase 1 (*CHAC1*, Hs00225520_m1), cystine/glutamate antiporter, solute carrier family 7 member 11 (*SLC7A11*, Hs00921938_m1), and glyceraldehyde-3-phosphate dehydrogenase (*GAPDH*, Hs99999905_m1, endogenous control; all from Thermo Fisher Scientific), using the TaqMan Fast Advanced Master Mix in QuantStudio 3 Real-Time PCR System (Thermo Fisher Scientific) according to the manufacturer's instructions with an elongated initial DNA denaturation time (95 °C for 2 min). Two separate experiments were conducted, including six technical replicates. Each technical replicate was analyzed in triplicate. qPCR data were normalized to *GAPDH* and analyzed with the $2^{-\Delta\Delta CT}$ method [28] for relative gene expression analysis.

Statistical analyses: For the permeability testing, the apparent permeability coefficient (P_{app}, cm/s) was calculated according to the following equation: $P_{app} = (\Delta Qr / \Delta t) / (C_d \times A)$, where $\Delta Qr/\Delta t$ is the slope of the linear region of the cumulative amount of the compound in the receiver chamber versus time plot, C_d is the average concentration of the compound in the donor chamber during the experiment, and A is the surface area of the insert (1.12 cm^2). Data are presented as mean ± standard deviation (SD).

The relative fluorescence unit (RFU) of background was measured and deducted from all treated and control conditions, and cell viability (% of control) was calculated with the following equation: $RFU_{treated}/RFU_{control} \times 100$. The four-parameter dose–response curve was fitted using GraphPad Prism (version 10.4.0; Dotmatics, Boston, MA) to obtain the half-maximal inhibitory concentration (IC_{50}), defined as the concentration of $NaIO_3$ that reduces cell viability to 50%. LDH and ROS data were normalized to the control condition (0 mM $NaIO_3$). LDH data were analyzed as a four-parameter dose–response curve, and the half-maximal effective concentration (EC_{50}) for the LDH assay was calculated in GraphPad Prism software. Data are presented as mean ± SD.

Relative qPCR data were normalized to the control condition (0 mM $NaIO_3$). Quantitative data were analyzed using descriptive statistics and presented as mean ± SD. Statistical analyses were performed using GraphPad Prism, and differences were considered statistically significant at the multiplicity-adjusted $p < 0.05$ level. For normally distributed data, comparisons between the groups were determined using one-way analysis of variance, followed by Dunnett's multiple comparison test or two-way analysis of variance with Šidák's multiple comparison test.

RESULTS

Characteristics of native human RPE phenotype were expressed in hiPSC-RPE cells: The fluorescence images of zonula occludens 1 and occludin revealed that both proteins were strongly expressed at cell–cell junctions, and the typical polygonal shape of the cells was also clearly visible (Figure 1A, B). TEM images showed that the cells possessed several typical characteristics of native RPE cells, such as apical microvilli and melanosomes at all maturation stages, I to IV (Figure 1C, D). Interestingly, we also observed that occludin consistently stained a dot-like region in the middle of each hiPSC-RPE cell (Figure 1B and Figure 2A). Previous studies have observed occludin localization in centrosomes of primary cilia during cortex development [29]. Here, we explored whether occludin (Figure 2A) is costained with primary cilia marker ARL13B (Figure 2B). Indeed, double immunostaining of hiPSC-RPE cells and DAPI counterstaining revealed colocalization of occludin and ARL13B (Figure 2C). Lastly, we immunostained the cells against RPE-specific 65 kDa protein (RPE65), which was also expressed in the hiPSC-RPE cells (Figure 2D). Taken together, these maturity markers confirm the full maturation of the hiPSC-RPE cells grown in inserts [30].

Melanosome density and maturation in hiPSC-RPE cells: The density and maturation level of melanosomes were evaluated from TEM images (Figure 3A). In total, melanosomes were counted from 24 hiPSC-RPE cells. Similarly, as reported by others [31,32], we found that mature melanosomes of stages III and IV were more predominant in hiPSC-RPE cells than immature melanosomes of stages I and II (Figure 3A,B).

hiPSC-RPE cells presented tight junction functionality and monolayer tightness: The TEER values of hiPSC-RPE cells were measured to confirm the integrity of the cell monolayer grown for 28 days in inserts. The results showed high values both before (481 ± 36 Ω × cm^2) and after the permeability testing (549 ± 34 Ω × cm^2). The permeability testing of the reference compounds from the basolateral to apical direction showed that the reference compound with high permeability, rhodamine B, had the high P_{app} value (18.9 ± 7.7 × 10^{-6} cm/s, n = 6), while the low-permeability marker, 6-carboxyfluorescein (2.1 ± 1.2 × 10^{-6} cm/s, n = 6), had a significantly lower P_{app} value, indicating a strong epithelial barrier with good discrimination between low- and high-permeability values.

$NaIO_3$-induced oxidative stress decreased cell viability, induced ROS and VEGFA production, and promoted anti-oxidative, proangiogenic, and pro-ferroptotic gene expression in hiPSC-RPE cells: Cell viability decreased when the hiPSC-RPE cells were treated with $NaIO_3$ for 24 h. A decrease in resazurin was observed at 5 mM $NaIO_3$ and reached its

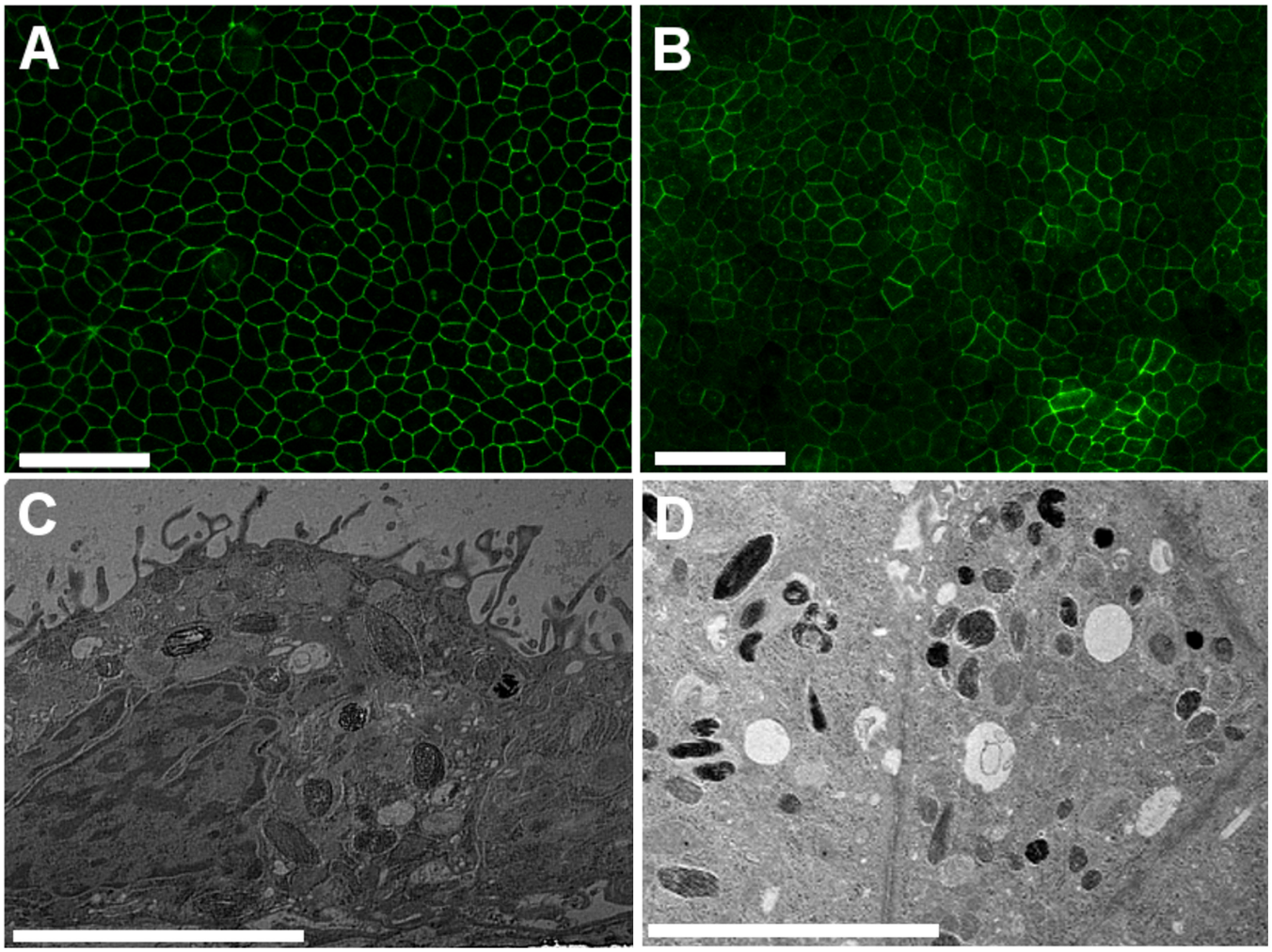


Figure 1. Characterization of tight junction protein expression, localization, and morphology in human induced pluripotent stem cell-derived retinal pigment epithelium. Representative immunofluorescence images of **A**: zonula occludens-1 (ZO-1) and **B**: occludin expression in human induced pluripotent stem cell-derived retinal pigment epithelium (hiPSC-RPE) monolayers. Representative transmission electron microscopy images showing **C**: vertical and **D**: horizontal cross-sections of the hiPSC-RPE monolayer. Scale bars: 50 µm (**A**, **B**) and 5 µm (**C**, **D**).

maximum at 20 mM, generating an IC_{50} of 9.4 mM (Figure 4A). Meanwhile, LDH levels started to rise with 3 mM $NaIO_3$ and rose steadily as the concentration increased to 10 mM $NaIO_3$, after which the LDH levels stayed stable despite increasing concentrations, resulting in an IC_{50} of 4.1 mM (Figure 4B). This indicates that $NaIO_3$ caused cell membrane damage first before affecting intracellular metabolism.

Interestingly, ROS formation was remarkably increased, even with the lowest $NaIO_3$ concentrations (0.1–2 mM; Figure 4A), while viability indicators did not show decreased cell viability. The ROS levels gradually decreased from 2 mM $NaIO_3$ onward, coinciding with the cell membrane damage indicated by LDH release (Figure 4B). In addition, an increase in VEGFA levels could already be seen with 1 mM $NaIO_3$ when the ROS levels peaked, and the VEGFA levels rose further to approximately 4 mM $NaIO_3$ (Figure 4B).

We sought to validate the principal cellular responses—cell viability, ROS generation, and the release of VEGFA—in hiPSC-RPE cells using an alternative oxidative agent, tBHP, which, although commonly used to induce oxidative stress in cellular models, is not specific to RPE cells. Compared with $NaIO_3$, tBHP produced a markedly steeper dose–response curve. The IC_{50} for resazurin reduction was 0.59 mM, while the EC_{50} for LDH release was 0.55 mM, indicating that tBHP induces intracellular metabolic impairment and cell membrane damage at approximately the same tBHP concentration (Figure 4C, D).

Interestingly, tBHP did not induce a comparable peak in ROS formation at lower concentrations of oxidative agent, in contrast to $NaIO_3$. Moreover, overall ROS levels were lower following tBHP induction (Figure 4C) than those observed with $NaIO_3$ (Figure 4A). Furthermore, VEGFA levels were elevated (Figure 4D), but the increase was less pronounced compared with $NaIO_3$ induction (Figure 4B).

Gene expression profiles of *VEGFA*, *HIF1A*, *TXN*, *TXNIP*, *CHAC1*, and *SLC7A11* were generated from $NaIO_3$-treated cells (Figure 5). The results revealed that *VEGFA*, *HIF1A*, *TXN*, *CHAC1*, and *SLC7A11* gene expression were significantly upregulated ($p < 0.05$), and *TXNIP* gene expression was significantly downregulated ($p < 0.05$) in cells treated with 2 to 6 mM $NaIO_3$ compared with untreated cells. Upregulation of the *TXN* gene, encoding thioredoxin, may lead to a reduction in ROS formation in hiPSC-RPE cells at 2 mM and higher concentrations of $NaIO_3$ (Figure 4A). Downregulation of the *TXNIP* gene (Figure 5D) may lead to an increase in VEGFA (Figure 4B). Oxidative stress induced upregulation of the ferroptosis mediator *CHAC1*, leading to enhanced glutathione degradation, mitochondrial dysfunction, and disruption of redox homeostasis (Figure 5E). Concurrently, increased expression of the cystine/glutamate antiporter (*SLC7A11*) gene at 2 mM $NaIO_3$ (Figure 5F) promoted cystine uptake and glutathione synthesis, which may represent an early adaptive response to mitigate oxidative stress and limit ferroptotic cell death.

Mn-TM-2-PyP–mediated antioxidant treatment suppressed $NaIO_3$-induced cytotoxicity in cell viability assays. The effect was less pronounced in the resazurin reduction-based cell viability assay, with a modest effect in the IC_{50} value shift from 9.0 to 11.5 mM (Figure 6A). In contrast, LDH release was markedly reduced, with a pronounced rightward shift in the EC_{50} from 5.1 to 11.0 mM (Figure 6B). Since gene expression changes were most pronounced at $NaIO_3$ concentrations of 4 to 6 mM across all genes tested (Figure 5), antioxidant effects were evaluated at these levels (Figure 6C–H). Antioxidant treatment consistently attenuated gene upregulation, reaching statistical significance for *VEGFA* and *TXN* at 4 and 5 mM $NaIO_3$ (Figure 6C, E). Notably, *TXNIP* gene expression was higher in antioxidant-treated cells exposed to 5 mM $NaIO_3$ than in untreated controls (Figure

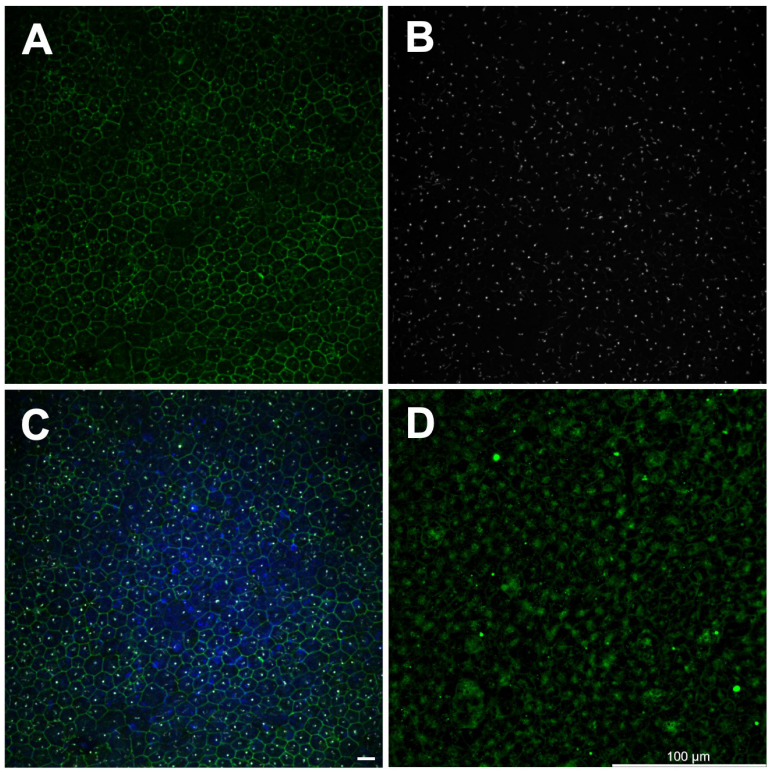


Figure 2. Assessment of maturity in human induced pluripotent stem cell-derived retinal pigment epithelium monolayers. Representative immunofluorescence images of human induced pluripotent stem cell-derived retinal pigment epithelium showing **A**: occludin, **B**: primary cilia (ARL13B), **C**: merged staining of occludin (green), primary cilia (grey), and DAPI (blue), and **D**: expression of the RPE maturity marker RPE65. Scale bars: 5 µm (**A**–**C**) and 100 µm (**D**).

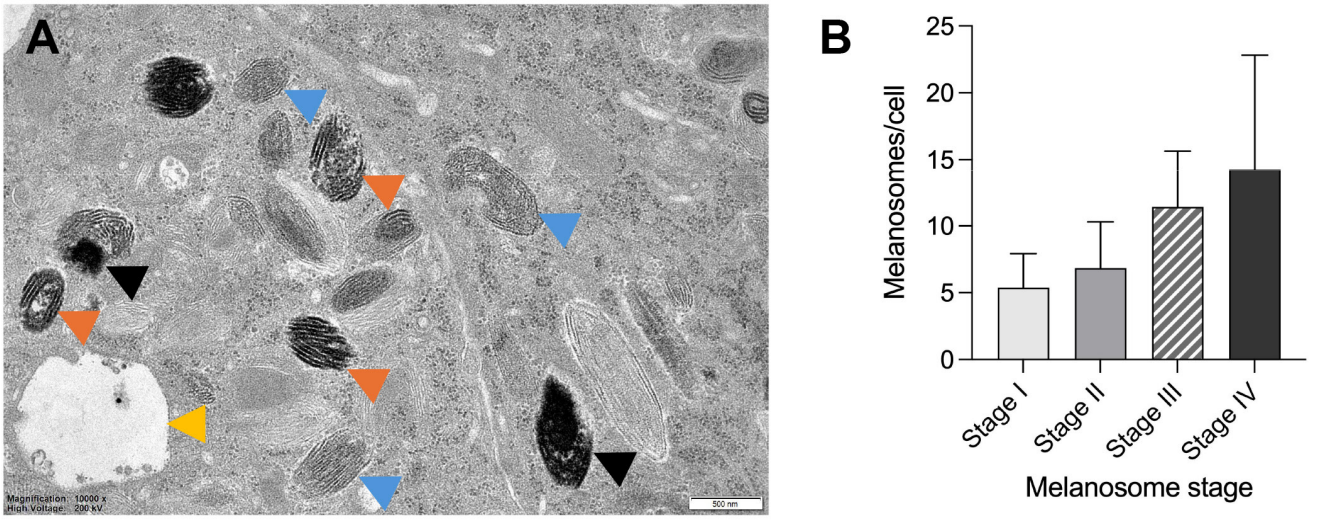


Figure 3. Melanosome density and maturation in human induced pluripotent stem cell-derived retinal pigment epithelium cells. **A**: Representative transmission electron microscopy image of human induced pluripotent stem cell-derived retinal pigment epithelium (hiPSC-RPE) cells containing immature melanosomes at stages I (yellow arrow) and II (blue arrow), and mature melanosomes at stages III (orange arrow) and IV (black arrow). Scale bar 500 nm. **B**: Number of melanosomes per hiPSC-RPE cell according to maturation stage. Data are presented as mean ± SD (n =24).

6F). These results suggest that antioxidant treatment helps to restore gene expression toward baseline in cells experiencing extensive oxidative stress. However, antioxidant-containing data should be interpreted as preliminary, and further replication is required to confirm these findings.

DISCUSSION

The aim of this study was to determine the response of hiPSC-RPE cells to $NaIO_3$-induced oxidative stress and study the activation of the thioredoxin antioxidant system by assessing the changes in the expression of antioxidative and proangiogenic-related genes. The first step in this study was to confirm that the hiPSC-RPE cells have the desired attributes, which were well documented previously [33,34]. The cells were monitored closely during culturing, and pigmentation could be seen approximately on day 15, which indicates the presence of functional melanogenesis. Immunofluorescent staining showed that the cell monolayer had contiguous tight junctional patterns, and several RPE characteristics, such as apical microvilli, melanosomes, and cuboidal epithelium morphology, could be seen in the TEM images. It was shown that mature melanosomes of stages III and IV were more predominant in hiPSC-RPE cells than immature melanosomes of stages I and II.

The functionality of hiPSC-RPE cell monolayer tight junctions was demonstrated by measuring TEER values. High TEER values observed were in agreement with the TEER values of fetal human RPE cell monolayer, as demonstrated by Ablonczy et al. [35], indicating that the cells had formed highly organized tight junctional complexes. Furthermore, high TEER values after permeability testing correlated with the low P_{app} value for the low-permeability reference molecule. Similarly, a low P_{app} value was previously reported in isolated bovine RPE-choroid [36]. The cells also displayed a barrier ~4 times tighter than that of the ARPE-19 cell line [37]. In the past, the ARPE-19 cell line was the most popular in vitro model of RPE. However, it has been shown that certain properties crucial for RPE cells, such as melanin pigment expression and monolayer tightness with functional tight junctions, are not properly represented in ARPE-19 cells [35]. The high P_{app} value for the high-permeability reference molecule and the low P_{app} value for the low-permeability reference molecule showed that the hiPSC-RPE cell monolayer discriminated between high and low values. This verifies that the cells provided epithelial polarity with a strong and tight paracellular barrier. The hiPSC-RPE cell monolayer maturity was further confirmed by the expression of primary cilia and RPE-specific maturity marker RPE65. Interestingly, we observed that occludin colocalized with the primary cilia. It has been shown that occludin is localized in the centrosomes of primary cilia during cortex development [32,38]. However, this has not been previously demonstrated in RPE cells, and therefore, further studies are needed to confirm if this is RPE cell specific or a general feature of primary cilia.

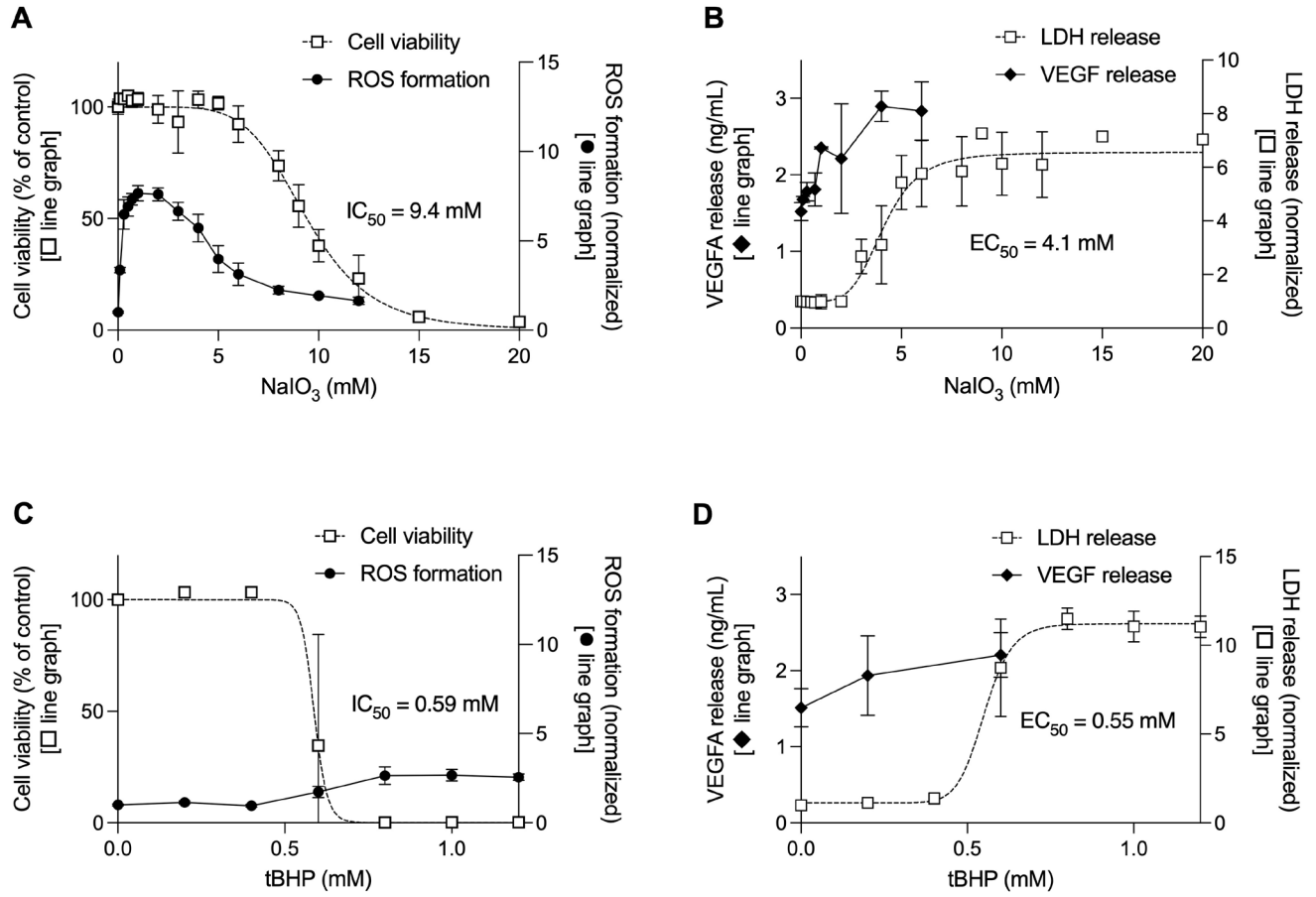


Figure 4. Cellular responses of human induced pluripotent stem cell-derived retinal pigment epithelium cells to 24 h $NaIO_3$- and tBHP-induced oxidative stress. **A**: Cell viability measured as intracellular reduction of resazurin and reactive oxygen species (ROS) formation after $NaIO_3$-induction. Cell viability is shown as a percentage of live cells compared to control cells. The half-maximal inhibitory concentration (IC_{50}) represents the concentration with which 50% of the cells died. **B**: Lactate dehydrogenase (LDH) and vascular endothelial growth factor A (VEGFA) release after $NaIO_3$-induction. The half-maximal effective concentration (EC_{50}) represents the concentration of $NaIO_3$ with which half of LDH maximum release was reached. **C**: Cell viability and ROS formation after tBHP-induction. **D**: LDH and VEGFA release after tBHP-induction. ROS and LDH levels were normalized control condition (0 mM). VEGFA release is shown as ng/ml. All data are shown as mean ± SD (n = 3).

Since we demonstrated that cells possessed all the required morphological and functional characteristics, we proceeded to explore oxidative stress–induced damage. However, it should be noted that the characterization tests were performed in cells grown on inserts while the oxidative stress experiments were performed on well plates. Thus, the culture conditions were not identical. As expected, treating the cells with $NaIO_3$ caused oxidative stress and induced hiPSC-RPE cell damage and death in a dose-dependent manner.

Intriguingly, $NaIO_3$ had increased intracellular ROS levels at the lowest tested concentrations, while viability indicators did not show decreased cell viability. ROS levels started to decrease when cell viability started to decrease. This may be a consequence of RPE-specific damage caused by $NaIO_3$.

Determining alterations in hiPSC-RPE gene expression showed that $NaIO_3$-induced oxidative stress upregulated *VEGFA*, *HIF1A*, and *TXN* expression. VEGFA is a growth factor that has a pivotal role in the pathogenesis of wet AMD as it promotes choroidal neovascularization, and its secretion increases with oxidative stress [8]. Therefore, upregulated *VEGFA* gene expression and increased VEGFA release observed in this study are in line with previous studies. The *TXN* gene encodes the thioredoxin protein, which has protective properties against oxidative stress. Thioredoxin

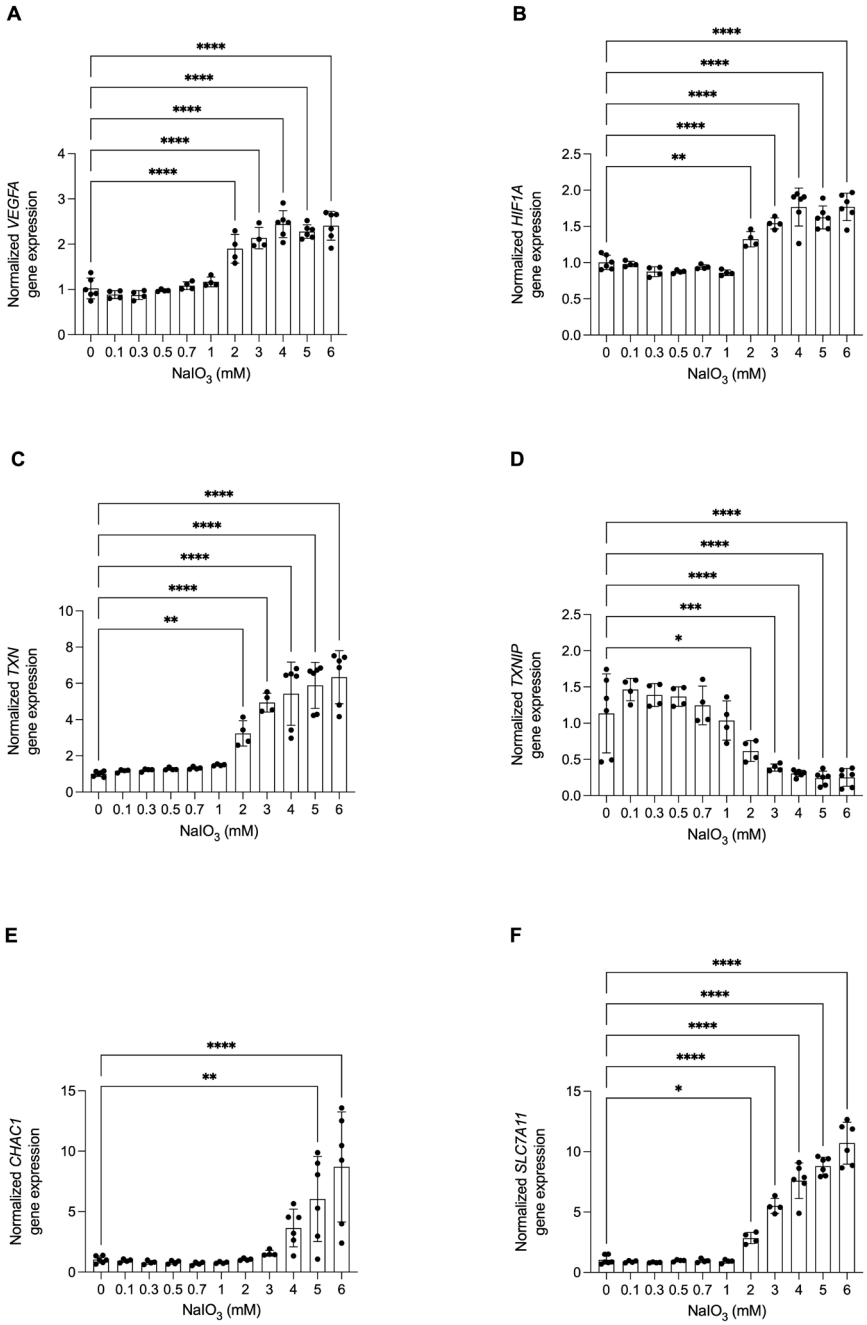


Figure 5. Gene expression profiles in human induced pluripotent stem cell-derived retinal pigment epithelium cells following 24 h $NaIO_3$-induced oxidative stress. Gene expression levels of **A**: Vascular endothelial growth factor A (*VEGFA*), **B**: Hypoxia-inducible factor 1-alpha (*HIF1A*), **C**: Thioredoxin (*TXN*), **D**: Thioredoxin interacting protein (*TXNIP*), **E**: Gamma-glutamylcyclotransferase 1 (*CHAC1*) and **F**: Cystine/glutamate antiporter (*SLC7A11*) were normalized to control condition. One-way ANOVA followed by Dunnett's multiple comparison test were performed for statistical analyses. *p < 0.05, **p < 0.01, ***p < 0.001, ****p < 0.0001. Each technical replicate is shown as a single data point with mean ± SD (n = 6).

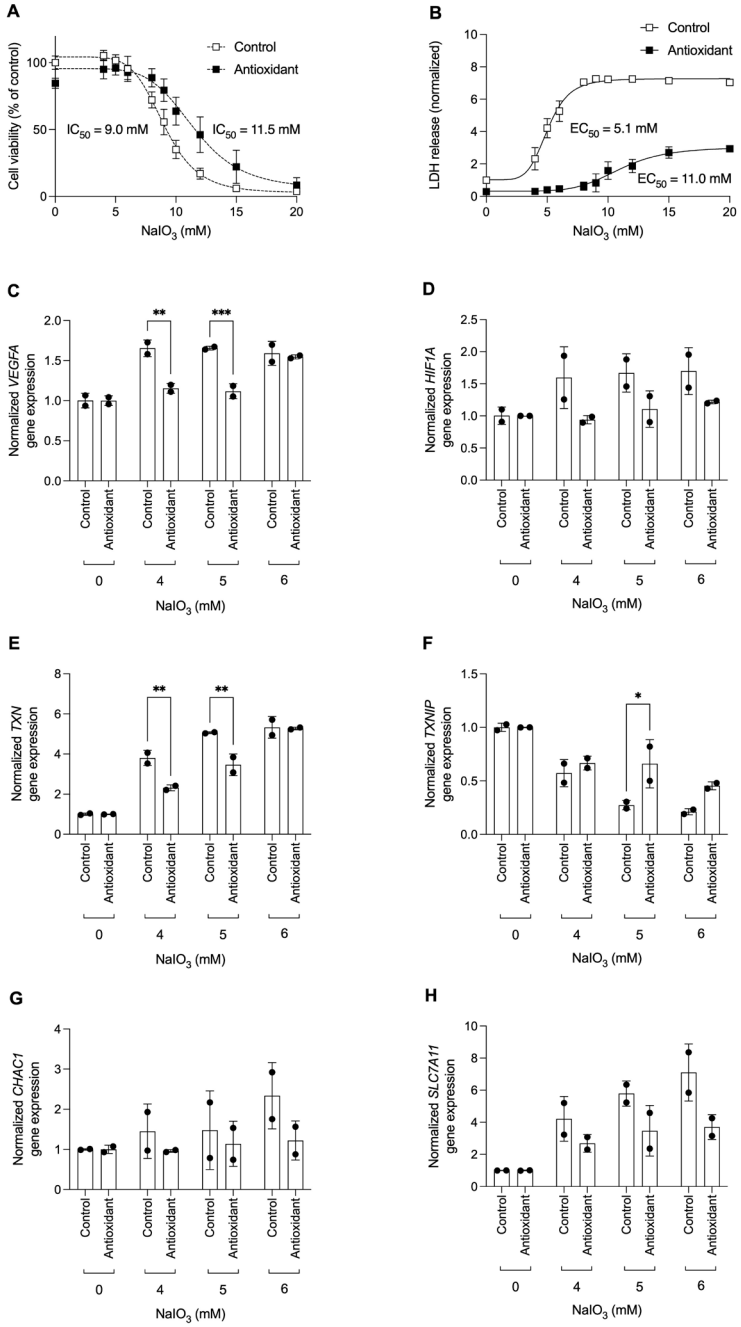


Figure 6. Antioxidant treatment suppresses $NaIO_3$-induced cytotoxicity and restore gene expression toward baseline in induced pluripotent stem cell-retinal pigment epithelium cells. Effect of $NaIO_3$ on hiPSC-RPE cell viability in the presence or absence of a broad redox-active antioxidant. Cells were pre-treated with Mn-TM-2-PyP (0.005%) for 24 h and during $NaIO_3$ exposure. **A**: Cell viability measured by intracellular resazurin reduction assay, expressed as a percentage relative to untreated control cells. The half-maximal inhibitory concentration (IC_{50}) indicates the $NaIO_3$ concentration causing 50% cell death. **B**: Cell viability assessed by lactate dehydrogenase (LDH) release. The half-maximal effective concentration (EC_{50}) represents the $NaIO_3$ concentration at which 50% of maximal LDH release was observed. Gene expression changes in the presence or absence of antioxidant at $NaIO_3$ concentrations of 4–6 mM. Expression of **C**: Vascular endothelial growth factor A (*VEGFA*), **D**: Hypoxia-inducible factor 1-alpha (*HIF1A*), **E**: Thioredoxin (*TXN*), **F**: Thioredoxin interacting protein (*TXNIP*). **G**: Gamma-glutamylcyclotransferase 1 (*CHAC1*) and **H**: Cystine/glutamate antiporter (*SLC7A11*) were normalized to control condition without antioxidant. Statistical analysis was performed using two-way ANOVA with Šidák's multiple comparison test. *p < 0.05, **p < 0.01, ***p < 0.001, ****p < 0.0001. Each technical replicate is shown as a single data point with mean ± SD (n = 2).

is known to decrease ROS levels and activate transcription factors, promoting cell viability in response to oxidative stress [16,39,40]. Upregulated *TXN* expression indicates that the thioredoxin system was activated only after exposure to 2 mM $NaIO_3$ and may have reduced ROS formation in hiPSC-RPE cells. HIF-1α, a transcription factor encoded by the *HIF1A* gene, regulates angiogenesis and mediates cellular response to reduced oxygen levels. HIF-1α expression increases in hypoxic conditions, upregulating VEGFA expression [41,42]. Lastly, we found that the *TXNIP* gene was downregulated at a 2 mM concentration of $NaIO_3$, and this downregulation was inversely proportional to all other studied genes. TXNIP protein promotes oxidative stress by inhibiting thioredoxin and various other factors [43]. These results are in line with a previous study by Cho et al., in which TXNIP was downregulated in ARPE-19 cells under oxidative stress. They also showed that knockdown of TXNIP increased HIF-1α expression and enhanced VEGFA secretion and angiogenesis in vitro [19]. Oxidative stress induced by $NaIO_3$, which selectively damages RPE cells, markedly modulated ferroptosis-related pathways, as demonstrated by the upregulation of *CHAC1* and *SLC7A11* genes. Upregulated *CHAC1* indicates activation of a pro-ferroptotic pathway through enhanced glutathione degradation, mitochondrial dysfunction, and disruption of redox homeostasis, thereby increasing susceptibility to lipid peroxidation. In parallel, elevated *SLC7A11* expression suggests an early adaptive response that promotes cystine uptake and glutathione synthesis to counteract oxidative damage. However, persistent oxidative stress and sustained *CHAC1* activity are likely to overwhelm this compensatory mechanism, ultimately favoring ferroptotic cell death. In this context, the downregulation of *TXNIP*, accompanied by increased *VEGFA* expression, may reflect a broader stress-adaptive response aimed at supporting cell survival despite progressive redox imbalance. Furthermore, Mn-TM-2-PyP–mediated antioxidant treatment seems to help restore gene expression toward baseline in cells experiencing extensive oxidative stress.

In this study, we demonstrated that hiPSC-RPE cells are morphologically and functionally similar to native RPE cells and are therefore well suited for nonclinical in vitro studies. At low $NaIO_3$ concentrations, ROS surged without compromising viability, enabling early detection of oxidative stress. This sensitivity allows screening of compounds targeting ROS-related pathways, such as *TXN* upregulation and *TXNIP* downregulation. This also mirrors AMD pathology, where oxidative stress drives VEGFA overexpression, making hiPSC-RPE cells ideal for testing antiangiogenic therapies (e.g., anti-VEGF drugs) and gene-editing therapies.

ACKNOWLEDGMENTS

The authors thank Associate Professor Soile Nymark from Tampere University, Tampere, Finland for imaging of the primary cilia with occludin, and Ville Jokinen (current affiliation National Bureau of Investigation, Finland) for imaging of the RPE65. We thank Mrs. Virpi Miettinen for assistance with TEM sample preparation and Dr. Jari Leskinen for his help conducting TEM imaging at the SIB Labs Kuopio Electron Microscopy Facility, part of the Department of Technical Physics of University of Eastern Finland and Biocenter Kuopio. Financial Disclosure statements No external funding sources were involved. All experiments were fully funded by Experimentica Ltd. Conflict of Interest GK is a founder, a shareholder and an executive chairman of Experimentica Ltd. JJH is an employee, a shareholder and a member of the board of Experimentica Ltd. Conference presentations The data was presented partially at The Association for Research in Vision and Ophthalmology ARVO 2024 (poster #194) and ARVO 2025 (poster #746) annual meetings.

This is an open-access article distributed under the terms of the Creative Commons Attribution-NonCommercial-NoDerivatives 4.0 International License, which permits reusers to copy and distribute the material in any medium or format in unadapted form only, for noncommercial purposes only, and only so long as attribution is given to the creator. CC BY-NC-ND includes the following elements: BY: credit must be given to the creator. NC: Only noncommercial uses of the work are permitted. ND: No derivatives or adaptations of the work are permitted.

REFERENCES

1. Gupta S, Lytvynchuk L, Ardan T, Studenovska H, Faura G, Eide L, Znaor L, Erceg S, Stieger K, Motlik J, Bharti K, Petrovski G. Retinal pigment epithelium cell development: Extrapolating basic biology to stem cell research. Biomedicines 2023; 11:310-[PMID: 36830851].
2. Strauss O. The retinal pigment epithelium in visual function. Physiol Rev 2005; 85:845-81. [PMID: 15987797].
3. Datta S, Cano M, Ebrahimi K, Wang L, Handa JT. The impact of oxidative stress and inflammation on RPE degeneration in non-neovascular AMD. Prog Retin Eye Res 2017; 60:201-18. [PMID: 28336424].
4. Boulton M, Dayhaw-Barker P. The role of the retinal pigment epithelium: topographical variation and ageing changes. Eye (Lond) 2001; 15:384-9. [PMID: 11450762].
5. Wong WL, Su X, Li X, Cheung CMG, Klein R, Cheng CY, Wong TY. Global prevalence of age-related macular degeneration and disease burden projection for 2020 and 2040: a systematic review and meta-analysis. Lancet Glob Health 2014; 2:106-16. [PMID: 25104651].

6. Heesterbeek TJ, Lorés-Motta L, Hoyng CB, Lechanteur YTE, den Hollander AI. Risk factors for progression of age-related macular degeneration. Ophthalmic Physiol Opt 2020; 40:140-70. [PMID: 32100327].

7. Sharma R, Bose D, Maminishkis A, Bharti K. Retinal pigment epithelium replacement therapy for age-related macular degeneration: Are we there yet? Annu Rev Pharmacol Toxicol 2020; 60:553-72. [PMID: 31914900].

8. Flaxel CJ, Adelman RA, Bailey ST, Fawzi A, Lim JI, Vemulakonda GA, Ying GS. Age-related macular degeneration preferred practice pattern®. Ophthalmology 2020; 127:1-65. [PMID: 31757502].

9. Pujol-Lereis LM, Schäfer N, Kuhn LB, Rohrer B, Pauly D. Interrelation between oxidative stress and complement activation in models of age-related macular degeneration. Adv Exp Med Biol 2016; 854:87-93. [PMID: 26427398].

10. Bellezza I. Oxidative stress in age-related macular degeneration: Nrf2 as therapeutic target. Front Pharmacol 2018; 9:1280-[PMID: 30455645].

11. Ruan Y, Jiang S, Gericke A. Age-related macular degeneration: Role of oxidative stress and blood vessels. Int J Mol Sci 2021; 22:1296-[PMID: 33525498].

12. Beatty S, Koh H, Phil M, Henson D, Boulton M. The role of oxidative stress in the pathogenesis of age-related macular degeneration. Surv Ophthalmol 2000; 45:115-34. [PMID: 11033038].

13. Liang FQ, Godley BF. Oxidative stress-induced mitochondrial DNA damage in human retinal pigment epithelial cells: a possible mechanism for RPE aging and age-related macular degeneration. Exp Eye Res 2003; 76:397-403. [PMID: 12634104].

14. Jager RD, Mieler WF, Miller JW. Age-related macular degeneration. N Engl J Med 2008; 358:2606-17. [PMID: 18550876].

15. Sohal RS, Orr WC. The redox stress hypothesis of aging. Free Radic Biol Med 2012; 52:539-55. [PMID: 22080087].

16. Lu J, Holmgren A. The thioredoxin antioxidant system. Free Radic Biol Med 2014; 66:75-87. [PMID: 23899494].

17. Nishiyama A, Matsui M, Iwata S, Hirota K, Masutani H, Nakamura H, Takagi Y, Sono H, Gon Y, Yodoi J. Identification of thioredoxin-binding protein-2/vitamin D(3) up-regulated protein 1 as a negative regulator of thioredoxin function and expression. J Biol Chem 1999; 274:21645-50. [PMID: 10419473].

18. Pan M, Zhang F, Qu K, Liu C, Zhang J. TXNIP: A double-edged sword in disease and therapeutic outlook. Oxid Med Cell Longev 2022; 2022:7805115[PMID: 35450411].

19. Ji Cho M, Yoon SJ, Kim W, Park J, Lee J, Park JG, Cho YL, Hun Kim J, Jang H, Park YJ, Lee SH, Min JK. Oxidative stress-mediated TXNIP loss causes RPE dysfunction. Exp Mol Med 2019; 51:1-13. [PMID: 31615975].

20. Shin D, Jeon JH, Jeong M, Suh HW, Kim S, Kim HC, Moon OS, Kim YS, Chung JW, Yoon SR, Kim WH, Choi I. VDUP1 mediates nuclear export of HIF1alpha via CRM1-dependent pathway. Biochim Biophys Acta 2008; 1783:838-48. [PMID: 18062927].

21. Zhang XY, Ng TK, Brelén ME, Wu D, Wang JX, Chan KP, Yung JSY, Cao D, Wang Y, Zhang S, Chan SO, Pang CP. Continuous exposure to non-lethal doses of sodium iodate induces retinal pigment epithelial cell dysfunction. Sci Rep 2016; 6:37279-[PMID: 27849035].

22. Liu B, Wang W, Shah A, Yu M, Liu Y, He L, Dang J, Yang L, Yan M, Ying Y, Tang Z, Liu K. Sodium iodate induces ferroptosis in human retinal pigment epithelium ARPE-19 cells. Cell Death Dis 2021; 12:230-[PMID: 33658488].

23. Yang X, Rai U, Chung JY, Esumi N. Fine tuning of an oxidative stress model with sodium iodate revealed protective effect of NF-κB inhibition and sex-specific difference in susceptibility of the retinal pigment epithelium. Antioxidants (Basel) 2021; 11:103-[PMID: 35052607].

24. Takahashi K, Tanabe K, Ohnuki M, Narita M, Ichisaka T, Tomoda K, Yamanaka S. Induction of pluripotent stem cells from adult human fibroblasts by defined factors. Cell 2007; 131:861-72. [PMID: 18035408].

25. Yu J, Vodyanik MA, Smuga-Otto K, Antosiewicz-Bourget J, Frane JL, Tian S, Nie J, Jonsdottir GA, Ruotti V, Stewart R, Slukvin II, Thomson JA. Induced pluripotent stem cell lines derived from human somatic cells. Science 2007; 318:1917-20. [PMID: 18029452].

26. Dalvi S, Galloway CA, Singh R. Pluripotent stem cells to model degenerative retinal diseases: The RPE perspective. Adv Exp Med Biol 2019; 1186:1-31. [PMID: 31654384].

27. Kaja S, Payne AJ, Singh T, Ghuman JK, Sieck EG, Koulen P. An optimized lactate dehydrogenase release assay for screening of drug candidates in neuroscience. J Pharmacol Toxicol Methods 2015; 73:1-6. [PMID: 25681780].

28. Livak KJ, Schmittgen TD. Analysis of relative gene expression data using real-time quantitative PCR and the 2(-Δ Δ C(T)) Method. Methods 2001; 25:402-8. [PMID: 11846609].

29. Bendriem RM, Singh S, Aleem AA, Antonetti DA, Ross ME. Tight junction protein occludin regulates progenitor Self-Renewal and survival in developing cortex. Elife 2019; 8:49376-[PMID: 31794381].

30. May-Simera HL, Wan Q, Jha BS, Hartford J, Khristov V, Dejene R, Chang J, Patnaik S, Lu Q, Banerjee P, Silver J, Insinna-Kettenhofen C, Patel D, Lotfi M, Malicdan M, Hotaling N, Maminishkis A, Sridharan R, Brooks B, Miyagishima K, Gunay-Aygun M, Pal R, Westlake C, Miller S, Sharma R, Bharti K. Primary cilium-mediated retinal pigment epithelium maturation is disrupted in ciliopathy patient cells. Cell Rep 2018; 22:189-205. [PMID: 29298421].

31. Aruta C, Giordano F, De Marzo A, Comitato A, Raposo G, Nandrot EF, Marigo V. In vitro differentiation of retinal pigment epithelium from adult retinal stem cells. Pigment Cell Melanoma Res 2011; 24:233-40. [PMID: 21232026].

32. Coutant K, Magne B, Ferland K, Fuentes-Rodriguez A, Chancy O, Mitchell A, Germain L, Landreville S. Melanocytes in

regenerative medicine applications and disease modeling. J Transl Med 2024; 22:336-[PMID: 38589876].

33. Maruotti J, Wahlin K, Gorrell D, Bhutto I, Lutty G, Zack DJ. A simple and scalable process for the differentiation of retinal pigment epithelium from human pluripotent stem cells. Stem Cells Transl Med 2013; 2:341-54. [PMID: 23585288].

34. Maruotti J, Sripathi SR, Bharti K, Fuller J, Wahlin KJ, Ranganathan V, Sluch VM, Berlinicke CA, Davis J, Kim C, Zhao L, Wan J, Qian J, Corneo B, Temple S, Dubey R, Olenyuk BZ, Bhutto I, Lutty GA, Zack DJ. Small-molecule-directed, efficient generation of retinal pigment epithelium from human pluripotent stem cells. Proc Natl Acad Sci U S A 2015; 112:10950-5. [PMID: 26269569].

35. Ablonczy Z, Dahrouj M, Tang PH, Liu Y, Sambamurti K, Marmorstein AD, Crosson CE. Human retinal pigment epithelium cells as functional models for the RPE in vivo. Invest Ophthalmol Vis Sci 2011; 52:8614-20. [PMID: 21960553].

36. Pitkänen L, Ranta VP, Moilanen H, Urtti A. Permeability of retinal pigment epithelium: effects of permeant molecular weight and lipophilicity. Invest Ophthalmol Vis Sci 2005; 46:641-6. [PMID: 15671294].

37. Mannermaa E, Reinisalo M, Ranta VP, Vellonen KS, Kokki H, Saarikko A, Kaarniranta K, Urtti A. Filter-cultured ARPE-19 cells as outer blood-retinal barrier model. Eur J Pharm Sci 2010; 40:289-96. [PMID: 20385230].

38. Wilsch-Bräuninger M, Huttner WB. Primary cilia and centrosomes in neocortex development. Front Neurosci 2021; 15:755867[PMID: 34744618].

39. Sugama K, Suzuki K, Yoshitani K, Shiraishi K, Miura S, Yoshioka H, Mori Y, Kometani T. Changes of thioredoxin, oxidative stress markers, inflammation and muscle/renal damage following intensive endurance exercise. Exerc Immunol Rev 2015; 21:130-42. [PMID: 25826051].

40. AlOkda A, Van Raamsdonk JM. Evolutionarily conserved role of thioredoxin systems in determining longevity. Antioxidants (Basel) 2023; 12:944-[PMID: 37107319].

41. Vadlapatla RK, Vadlapudi AD, Mitra AK. Hypoxia-inducible factor-1 (HIF-1): a potential target for intervention in ocular neovascular diseases. Curr Drug Targets 2013; 14:919-35. [PMID: 23701276].

42. Cheng L, Yu H, Yan N, Lai K, Xiang M. Hypoxia-inducible factor-1α target genes contribute to retinal neuroprotection. Front Cell Neurosci 2017; 11:20-[PMID: 28289375].

43. Choi EH, Park SJ. TXNIP: A key protein in the cellular stress response pathway and a potential therapeutic target. Exp Mol Med 2023; 55:1348-56. [PMID: 37394581].

Articles are provided courtesy of Emory University and The Abraham J. & Phyllis Katz Foundation. The print version of this article was created on 20 September 2026. This reflects all typographical corrections and errata to the article through that date. Details of any changes may be found in the online version of the article.